Published as: Bégin, P. N., Tanabe, Y., Kumagai, M., Culley, A. I., Paquette, M., Sarrazin, D., Uchida, M., and Vincent, W.F. 2020. Extreme warming and regime shift toward amplified variability in a far northern lake. Limnology and Oceanography **65**, doi:10.1002/lno.11546.

Extreme warming and regime shift toward amplified variability in a far northern lake

Paschale N. Bégin[1,2], Yukiko Tanabe[3,4], Michio Kumagai[5], Alexander I. Culley[1,6], Michel Paquette[1,7], Denis Sarrazin[1], Masaki Uchida[3,4] and Warwick F. Vincent[1,2]

Affiliations

[1]Centre d'études nordiques (CEN) & Takuvik Joint International Laboratory, Quebec City, Quebec, Canada

[2]Département de biologie, Université Laval, Quebec City, Quebec, Canada

[3]National Institute of Polar Research, Tachikawa, Japan

[4]The Graduate University for Advanced Studies, SOKENDAI

[5]Ritsumeikan University, Kyoto, Japan

[6]Département de biochimie, de microbiologie et de bio-informatique, Université Laval, Quebec City, Quebec, Canada

[7]Department of Geography and Planning, Queen's University, Kingston, Ontario, Canada

Correspondence

Corresponding authors:

Paschale N. Bégin paschale-noel.begin.1@ulaval.ca ORCID: 0000-0002-1031-3559

Warwick F. Vincent warwick.vincent@bio.ulaval.ca ORCID: 0000-0001-9055-1938

Co-authors:

Yukiko Tanabe ukkopu@gmail.com

Michio Kumagai mkt24354@se.ritsumei.ac.jp

Alexander I. Culley alexander.culley@bcm.ulaval.ca

Michel Paquette mp153@queensu.ca

Denis Sarrazin denis.sarrazin@cen.ulaval.ca

Masaki Uchida uchida@nipr.ac.jp

Running head: Arctic lake responses to extreme warming

Keywords: climate change, polar, oxygen, winter limnology, ice cover

Submitted to *Limnology and Oceanography* special issue "Arctic aquatic ecosystems in the 21st century" edited by Peter Hernes, Suzanne Tank and Ronnie N. Glud

Abstract

Mean annual air temperatures in the High Arctic are rising rapidly, with extreme warming events becoming increasingly common. Little is known, however, about the consequences of such events on the ice-capped lakes that occur abundantly across this region. Here we compared two years of high-frequency monitoring data in Ward Hunt Lake in the Canadian High Arctic. One of the years included a period of anomalously warm conditions that allowed us to address the question of how loss of multi-year ice cover affects the limnological properties of polar lakes. A mooring installed at the deepest point of the lake (9.7 m) recorded temperature, oxygen, chlorophyll *a* fluorescence and underwater irradiance from July 2016 to July 2018, and an automated camera documented changes in ice cover. The complete loss of ice cover in summer 2016 resulted in full wind exposure and complete mixing of the water column. This mixing caused ventilation of lake water heat to the atmosphere and 4 °C lower water temperatures than under ice-covered conditions. There were also high values of chlorophyll *a* fluorescence, elevated turbidity and large oxygen fluctuations throughout fall and winter. During the subsequent summer, the lake retained its ice cover and the water column remained stratified, with lower chlorophyll *a* fluorescence and anoxic bottom waters. Extreme warming events are likely to shift polar lakes that were formerly capped by continuous thick ice to a regime of irregular ice loss and unstable limnological conditions that vary greatly from year to year.

Introduction

The Arctic is experiencing climate warming at a two to three times faster rate than other parts of the planet (Meredith et al. 2019), and its ice-dependent ecosystems are especially vulnerable to this accelerated change. Major shifts are occurring in the Arctic cryosphere such as thinning of the sea ice (Babb et al. 2019), reduction of the sea ice albedo via the alteration of its surface (Landy et al. 2015), decreases in sea ice area and duration (Babb et al. 2019), negative mass balance of glacial ice (Overland et al. 2019), thawing of permafrost (Schuur et al. 2015), reduction of snow cover area and duration (Mudryk et al. 2018) and loss of lake ice cover (Wrona et al. 2016), with wide-ranging effects on north polar ecosystems (Macias-Fauria and Post 2018; Vincent 2020). This warming is associated with not only higher mean temperatures, but also increased variability within and between years.

Extreme heating events in the Arctic regions have occurred more frequently during the past decades, including in Alaska (Bieniek and Walsh 2017). Persistent high temperatures during such periods have the potential to affect lake hydrology and ecology (Lehnherr et al. 2018), as well as limnological dynamics during the subsequent seasons (Hampton et al. 2017). Arctic lakes are characterized by the presence of a thick ice cover that persists for most of the year. This ice limits gas exchanges between the water column and the atmosphere, and prevents direct wind-induced mixing, resulting in a stratified water column beneath the ice and oxygen to be drawn down over winter (Schindler et al. 1974). The ice cover reduces the penetration of solar radiation into the water column, especially when capped by reflective white ice or snow (Belzile et al. 2001). However, the solar energy penetrating the ice can slowly warm parts of the water column to well above ambient air temperatures. As an example, water temperatures reaching 8.5°C were observed in a High Arctic meromictic lake, and were likely the result of many decades of energy accumulation beneath the ice (Vincent et al. 2008). This solar heating can drive convective mixing cells (Kirillin et al. 2012; Pernica et al. 2017), and the photosynthetically available radiation (PAR) entering the water column can be sufficient to support photosynthesis below the ice, leading to oxygen supersaturation (Ludlam 1996). However, measurements are generally limited to summer and to regions where the ice cover melts out each year, and little is known about the seasonal variations in water temperature, oxygen, primary productivity and light in perennially ice-covered Arctic lakes, especially in fall and spring when critical transitions are likely to occur (Hampton et al. 2017; Matveev et al. 2019). Annual under-ice records are lacking in most Arctic regions, and especially in the High Arctic due to logistical constraints.

Ward Hunt Lake, Canada's northernmost lake, was characterized by 4 m-thick perennial ice cover over a 50-year record, followed by a period of rapid thinning and full loss of ice in summer 2011 and 2012 (Paquette et al. 2015). The aims of the present study were to evaluate the end-of-season dynamics during the new regime of intermittent ice-out and to obtain the first winter records for this lake. Two contrasting summers, with and without ice cover, allowed us to address the hypothesis that the shift in polar lakes from a continuous ice regime in the past to intermittent ice-out is accompanied by large scale variations in limnological properties such as water temperature, underwater PAR, phytoplankton variables (in this study, chlorophyll *a* fluorescence) and dissolved oxygen. Our results provide insight into how polar lakes elsewhere, for example lakes in Antarctica that are projected to lose their ice covers in the decades ahead (Obryk et al. 2019), will respond to extreme warming events.

METHODS

Study site

Ward Hunt Lake is located 26 m above sea level on Ward Hunt Island, 6 km off the northern coast of Ellesmere Island, within Quttinirpaaq National Park, Nunavut, Canada (Supporting Information Fig. S1). Its maximum known depth is 9.7 m, with a length of 990 m and an area of 0.37 km^2. The lake is mainly supplied by snow meltwater from the watershed via surface and subsurface water tracks, and drains to the sea by an outflow at its southern shore. The Ward Hunt Lake watershed and its water track hydrology are described in Paquette et al. (2017), and environmental features of the region are described in Vincent et al. (2011). The island experiences a polar desert climate, with a mean annual temperature of -17.4 °C (CEN 2020) and mean annual precipitation likely similar to that recorded at Alert, 170 km to the south-east (mean of 155 mm for the period 1951–2017; Environment Canada, data available at http://climate.weather.gc.ca). A meteorological station in the SILA Network operated by the Center for Northern Studies (CEN) is located 1 km north of Ward Hunt Lake, and during the period of study it recorded air temperature (thermistor HMP35CF, Vaisala, Helsinki, Finland, protected with a multi-plate radiation shield model 41003, R.M. Young Co., MI), incident solar radiation (radiometer LI-200, Li-Cor Biosciences, NE, USA), wind speed and direction (Wind Monitor 05103-10, R.M. Young Co., MI) and snow height (Sonic Ranging Sensor SR50, Campbell Scientific, UT, USA) every hour; these data are archived in CEN (2020). Melting degree days (MDD) were calculated as the sum of mean daily air temperatures above 0 °C each spring and summer (May to September). Freezing degree days (FDD) were calculated as the sum of mean daily air temperatures below 0 °C from July of the previous year to June of the listed year, spanning the complete winter period.

Year-round lake observations

A mooring system was installed from 20 July 2016 to 19 July 2018 at the deepest point of Ward Hunt Lake (83°05.226'N; 74°08.721'W; WGS84 map datum). It was equipped with sensors to record: dissolved oxygen saturation and temperature (O_2 and T°; MiniDO$_2$T, PME, CA, USA; oxygen resolution: 0.01 mg L^{-1}, temperature resolution: 0.01 °C); photosynthetically active radiation (PAR; ALW-CMP, JFE Advantec, Japan; PAR resolution: 0.1 µmol m^{-2} s^{-1}); chlorophyll *a* fluorescence (Chl *a*;

ACLW-CMP, JFE Advantec, Japan; resolution: 0.01 µg L^{-1}) and additional temperature measurements (T°; Minilog-II-T, Vemco, NS, Canada; DEFI-T, JFE Advantec, Japan; temperature resolution: 0.01 °C). The sensors were calibrated by the manufacturers, and maintenance and cleaning were performed each year at the time of data recovery and battery replacement. The chlorophyll *a* optical sensor was equipped with a wiper that was activated before each measurement, and the recorded concentrations were compared with extracted chlorophyll *a* analyses of samples taken at the same depth during field visits each year. Water for these pigment extractions was filtered through 25 mm GF/F filters that were stored at -80 °C until analysis. The pigments were extracted with 95% methanol and measured by high pressure liquid chromatography (HPLC) as in Bonilla et al. (2005).

Sensors were installed at nine subsurface depths (relative to the piezometric water surface): 2.8 m (PAR, T°), 3.8 m (T°), 4.8 m (T°), 5.8 m (Chl *a*, T°), 6.9 m (T°), 7.9 m (T°), 8.5 m (O_2, PAR, T°) and 9.0 m (T°). In 2017, two oxygen sensors were installed at 3.8 m and 5.8 m, the deep oxygen sensor was moved to 9.3 m and combined with a logging CTD (RBR420, RBR Ltd., ON, Canada), and all the other sensors were retained at the same depths. The logging frequency was set to 10 min for the temperature loggers, 30 min for the PAR and Chl *a* loggers and 60 min for the CTD. The logging frequency for the dissolved oxygen sensor was set to 1 min from 20 July 2016 to 22 January 2017 and to 1 hour from 15 July 2017 to 19 July 2018. The loggers were installed along a chain held upright from an anchor on the sediments to a float at the top. The mooring was designed so that the float was always below the ice to prevent any displacement of the mooring by movements of the ice cover.

The chlorophyll *a* fluorescence sensor was installed at 5.8 m. This depth was chosen because it was at the middle of a convective mixing zone from 4 to 8 m that had been detected in previous years of sampling (Mohit et al. 2017) as well as in the present study (Supporting Information Fig. S2), and was a stratum with supersaturated oxygen levels, indicative of active phytoplankton populations. Net oxygen gain or loss rates were calculated by fitting a linear regression model to oxygen concentrations and saturation values as a function of time during periods of linear change (identified visually from the time series plots) from mid-July to the end of October in each year. Differences in these slopes between 2016 and 2017 in the lower water column and between depths in 2017 were tested with a set of ANCOVA analyses.

Time-lapse images of Ward Hunt Lake were captured at hourly intervals from 04:00 to 19:00 h each day with an automated camera to couple limnological measurements of change with ice and snow events. Details of this camera installation and the full data set of images are archived in NEIGE (2020). To compare incident solar radiation (in W m^{-2}) with PAR in the water column (in µmol photons m^{-2} s^{-1}), we applied a factor of 4.57 (Sager and McFarlane 1997). Incident radiation was measured from 400 to 1100 nm, and we therefore also applied a factor of 0.55 which corresponds to the proportion of energy contained in the range of PAR (400–700 nm) using the relationship $E=h*c/w$, where E corresponds to the energy in joules, h=6.626×10^{-34} J s (Plank's constant), c=2.998×10^{8} m s^{-1} (speed of light), and w corresponds to the wavelength (m). Diffuse attenuation coefficients (K_d) were calculated from the underwater PAR values with the equation $K_d=-\ln(E_2/E_1)/(z_2–z_1)$, where E_1 was the irradiance recorded by the top sensor (z_1=2.8 m) and E_2 was the irradiance recorded by the bottom sensor (z_2=8.5 m).

RESULTS

Thermal and ice regime

The mean annual air temperature at Ward Hunt Island in 2016 was -15.6 °C, whereas the 2003–2017 mean was -17.4 °C (Supporting Information Table S1). This translated into 196 melting degree days (MDD) in 2016, which was the highest value ever recorded at Ward Hunt Island, and 77% above the overall mean MDD for the period 2003-2017 (Fig. 1). At Alert, which has a much longer meteorological record, the mean annual temperature in 2016 was -13.8 °C whereas the 1951–2017 mean was -17.5 °C (Supporting Information Table S2). Since 1990, there has been a significant overall linear trend of increasing annual MDD (on average, by 40 per decade), but with large year-to-year fluctuations (Fig. 1; for 1990 to 2017, linear regression r^2=0.16, *F*=6.1, df=26, *p*=0.02). The annual MDD in 2016 totaled 439, more than three standard deviations (108%) above the 1951–2017 mean which was 210 (Fig. 1). The mean annual air temperature value at Alert for 2016 was the maximum for the entire 67-year record (Supporting Information Table S2). For the period of overlap, these two MDD records were highly correlated (Pearson's correlation test, *r*=0.97, df=13, *p*<0.001), with Ward Hunt values averaging 134 fewer MDD than Alert. Freezing degree days at Ward Hunt Island from July 2016 to June 2017 totaled 6054, which was more than one SD below the 2003–2017 mean (6470; Supporting Information Table S1). The freezing degree days value at Alert was 5679, more than two SD below the mean of 6597 (Supporting Information Table S2).

Water temperatures reached 6.6°C at the bottom of Ward Hunt Lake at the end of July 2016 (Fig. 2a,b; Supporting Information Fig. S3), likely due to the warmest air temperatures (up to 7 °C) at this time, combined with highest irradiances under the thinning ice (1.80 m of ice cover on 14 July 2016 versus 2.18 m thickness on 14 July 2015). At the time of our visit in mid-July, there was already a distinct moat of open water along the northern and western edge of the lake, which subsequently widened (Fig. 3a). The water column showed an inverse thermal stratification by the end of summer 2016. The profiles in July 2016 were strongly influenced by salinity gradients; water at 4 °C with a lower conductivity was located above warmer, higher conductivity water towards the bottom (Supporting Information Fig. S2). This stratification persisted until July 27 when the camera showed that the ice cover had become detached from the edge of the lake and was moving north-eastwards due to strong winds from the south-west at that time (Supporting Information Fig. S4), which likely resulted in associated water movements beneath the ice cover. The water depth recorded via the pressure sensor on the logging CTD from July 2017 to July 2018 showed small-scale fluctuations (root-mean-square error of 0.097 m), with a mean increase of 0.28 m over this period (Supporting Information Fig. S5).

The automated camera recorded complete loss of the lake ice on 16 August 2016 (Fig. 3b). The water column was then exposed to wind and was mixed completely, with a subsequent drop in water temperatures to near 0 °C in the whole water column. The lake returned to the pattern of inverse thermal stratification under the ice in November 2016, which persisted throughout winter. Water temperatures warmed during summer 2017, to around 6 °C throughout much of the ice-covered water column by early August (Figs 2 and 3). The striking difference between ice-covered 2017 and ice-free 2016 is illustrated in the central panels of Fig. 3, showing that August-September bottom water temperatures were 2-4 °C warmer in 2017.

Light and chlorophyll fluorescence

Ward Hunt Island experiences extreme polar winters with a total absence of solar radiation from mid-October to March (Fig. 2c,d). The lake was covered by ice for most of the period of observation, and the resultant effect on underwater light was compounded by snow cover in spring and intermittent snowfall over the ice in summer (Fig 3f). As a result of the combined effects of snow, ice and the seasonality of incident radiation, the main period of PAR availability in the water column was July-August (Fig. 4a,b,c).

There was a pronounced difference in the underwater light regime between the two years. The 1-year ice derived from freeze-up in winter 2016/17 allowed light to penetrate into the water column in April 2017, whereas the 2-year ice derived from the winters of 2016/17 and 2017/18 (and associated snow cover) delayed the rise in underwater PAR to June 2018 (Figs 4b,c). Comparing with the algal physiological and growth thresholds identified by Gosselin et al. (1985), PAR in the upper water column reached 7.6 µmol m^{-2} s^{-1} (photosynthetic activity threshold) on 18 May 2017 and 20 µmol m^{-2} s^{-1} (biomass accrual threshold) on 7 June 2017. In contrast, the spring 2018 irradiance in the upper water column was less than 0.5 µmol m^{-2} s^{-1} through May, the photosynthetic activity threshold value was not achieved until 29 June, and the biomass accrual threshold not until 3 July, about one month later than in 2017.

The lower irradiance conditions at the bottom of the lake during the mixing period of August 2016 were not associated with lower irradiance at the surface (Fig. 4b,c), but were the result of increased attenuation through the water column, as measured by the sharply increased K_d values relative to August 2017 (Fig. 5a), Chlorophyll *a* fluorescence values increased during this period (Fig. 4d), and were positively correlated with K_d (Pearsons' correlation test r=0.37, df=1396, p<0.001). In contrast, the large difference in bottom PAR between the May-July period in 2017 and 2018 (Fig. 4b,c) was at a time of similar incident irradiance and K_d attenuation coefficients (Fig. 5b). However, snow accumulation on the ice cover was 12-20 cm thick in mid-July 2018 but absent in the other years of sampling, and the resultant differences in reflection and attenuation likely produced this 2017 versus 2018 divergence in underwater PAR.

Two peaks in in vivo chlorophyll *a* fluorescence in the mid water column occurred in both years, with one in spring and the second in late summer. The maximum (Fig. 2e) and mean daily (Fig. 4d) fluorescence values in September 2016 were around 50% higher than in the subsequent ice-covered year, and occurred earlier in 2016, near the end of the period of ice-out and full water column mixing. The spring rise in chlorophyll *a* fluorescence began much earlier in 2017 (mid-April) than in 2018 (mid-June), reflecting the earlier rise in PAR beneath the 1-year versus 2-year ice cover; this was also indicated by the earlier rise in water column K_d values in 2017 (Fig. 5b). Peak fluorescence was timed at least 2 weeks earlier in 2017 than in 2018 (Figs 2e, 4d), and corresponded to a period of sharply reduced under-ice irradiance (Fig. 4b,c) associated with a period of snowfall over the ice at that time (Supporting Information Fig. S6). The high PAR penetration in the water column in late June and early July 2017 were likely associated with the melting and loss of snow over the ice. Comparison of chlorophyll *a* concentrations as measured by the fluorescence sensor with those obtained by HPLC analysis of sample extracts showed a close match on all three dates, with a small mean difference of 0.17 µg L^{-1} (Fig. 2e), and no evidence of sensor drift.

Dissolved oxygen

Oxygen rose in concentration in the lower water column of Ward Hunt Lake during the summer ice-covered period, to a maximum of 140 % saturation (% air-equilibrium value at the measured water temperature) in both years. However, there was a faster rate of increase above saturation at the end of July 2016 (5.31 % d^{-1}) than in the period late July to mid-August 2017 (2.48 % d^{-1}; Table 1; Fig. 3, in red). There were high frequency oscillations in temperature and dissolved oxygen at the bottom of the lake during the 2016 ice-covered period, indicative of internal waves with a period of 110 mins (Supporting Information Fig. S7). With the movement and break-up of the ice cover in late July-August 2016, and water column mixing and ventilation under the influence of strong winds (Supporting Information Fig. S4), dissolved oxygen saturation dropped at a rate of -2.30 % d^{-1}. Oxygen values subsequently remained around 100% saturation (change rate of 0.08 % d^{-1}) until freeze-up and the reinstatement of ice cover in September.

After a two-week delay, dissolved oxygen then decreased (-3.03 % d^{-1}) to undetectable levels by late November 2016. Fluctuations in oxygen were observed over the subsequent two months until the logger reached its memory capacity in late January and ceased recording. In 2017, water oxygen concentrations at 9.3 m followed a contrasting pattern, with values above 100% through most of August and a maximum value that was higher and later than in the previous year (Fig. 3, right panel). From mid-August 2017 onwards, oxygen concentrations in the lower water column steadily decreased, and then much more rapidly in early September (Table 1). The lower water column became anoxic by the end of September, two months earlier than in 2016. It remained anoxic while the middle of the water column remained at 50% of oxygen in the upper water column at saturation for the rest of the record until July 2018, when oxygen saturation increased in the middle water column (5.10 % d^{-1}) in tandem with increasing chlorophyll *a* fluorescence.

Comparison of the net oxygen change rates in absolute units indicated a period of high variability from 20 July to the end of September in both years (Table 2). However, the timing of the shift from positive to negative oxygen balance differed between years: this was late August in 2017, but around one month later (late September) in 2016. The installation of the additional two oxygen sensors for the second year showed that net oxygen change rates were of larger amplitude and more variable in the lower water column relative to the shallower depths. Highest rates of net oxygen accumulation in the bottom waters occurred in late July in both years, but in 2017 this high positive rate continued into mid-August and then became strongly negative, with a net depletion rate exceeding 1000 mg O_2 m^{-3} d^{-1}. This depletion rate was around twice the maximum oxygen loss rate measured in 2016, and occurred while the ice cover remained in the first half of September, whereas in 2016 maximum depletion rates occurred while the ice cover was gradually reforming in the second half of September (Figure 2). The ANCOVA analyses of the linear regression slopes showed that the bottom water oxygen change rates were significantly different (p<0.05) between 2016 and 2017 for every equivalent 14-day period in Table 2.

Discussion

The northern coastline of Ellesmere Island experienced extreme warming in 2016, with record maximum air temperatures and an unusually high number of melting degree days at Ward Hunt Island and Alert. These elevated temperatures appear to be part of a broader pattern of warming that extended across the central Arctic earlier that year (Overland et al. 2019). The following year, the northern Ellesmere Island region returned to much cooler conditions that persisted throughout summer. These contrasting temperature regimes resulted in striking differences in the ice cover of Ward Hunt Lake, and consistent with the hypothesis that an unstable ice regime results in largescale variations in limnological properties, we recorded major differences between the two summers in temperature and mixing, underwater light, chlorophyll *a* fluorescence and oxygen dynamics. Some of these differences continued into fall and winter, for example net oxygen depletion rates, in accordance with our hypothesis that intermittent ice-out causes limnological effects that extend beyond the open water period. Extreme warming events are likely to increase in intensity and duration with ongoing global climate change (Meredith et al. 2019), and our two-year comparison of high frequency observations from Ward Hunt Lake provides insights into the future state of polar aquatic ecosystems.

Ice cover

A major transition in the lake ice regime of Ward Hunt Lake has taken place over the last two decades, with the rapid thinning of its summer ice cap from a thickness around 4 m in 2003 to the first loss of ice and open water conditions in 2011 (Paquette et al. 2015). The thinner summer ice has contributed to an enhanced sensitivity to climate warming, with full ice-out occurring subsequently in 2012 and 2016. These changes are consistent with the general contraction of the cryosphere, including a shorter duration of lake ice cover in the Arctic (Du et al. 2017) and more generally throughout the Northern Hemisphere (Sharma et al. 2019).

The transition from perennial to annual lake ice cover implies not only less ice, but also a greater degree of interannual variability in ice conditions. This effect has been observed and modeled for Arctic sea ice, where the replacement of thick multiyear ice by annual ice results in a greater response to year-to-year variations in climate forcing (Serreze and Meier 2019). This is because less energy is required to completely melt the ice, and also because wider expanses of open water result in positive feedback effects that amplify the interannual variations in ice melt (Mioduszewski et al. 2019). For Ward Hunt Lake, the transition to a more extensive moat each year increases not only the solar heating of the lake, but also allows the central ice pan to detach from the shore and move around, as seen in the late summer images in both years (NEIGE 2020). This movement of the ice cover increases its likelihood of mechanical break-up of the ice, and allows greater exposure of ice surfaces to warmer littoral water. The thinning of the ice combined with more rapid loss of overlying snow also results in a greater penetration of solar energy to warm the underlying water column.

Projections of temperature and ice changes in permanently ice-covered Lake Bonney, Antarctica, indicate that this lake will lose its 3-5 m ice cap within one to four decades, with an abrupt shift from multiyear to annual ice cover (Obryk et al. 2019). The results from Ward Hunt Lake show that such changes in polar lakes may not be a simple transition from always ice-covered to annually ice-free, but rather there may be a new regime, as observed here, of alternating periods of multiyear and annual ice conditions due to the amplified sensitivity of thin ice to interannual variability in climate. This type of year to year variation was also noted during the IBP study of High Arctic Char Lake (Schindler et al. 1974), which lies 1000 km to the south of Ward Hunt Island. In three of the four study years, the lake experienced open water conditions in late August, but during a cold cloudy summer the lake remained ice-covered, and the 2-year ice accumulated to 2.9 m thickness by May the next year. Even lakes that are continuously overlaid by thick ice are known to respond to climate signals (Fountain et al. 2016), however the transition to thin ice that can completely melt out in warmer years results in a new regime of amplified sensitivity to climate fluctuations.

Mixing and stratification

Consistent with our hypothesis, the ice-out conditions in Ward Hunt Lake induced by extreme warming during August-September 2016 resulted in a completely different thermal regime than in the subsequent year of sustained ice cover. The exposure of the water column to convective cooling as well as direct wind-induced mixing in 2016 resulted in uniform temperatures throughout the water column and loss of energy to the overlying atmosphere. This effect was observed at Char Lake when a fall period of open water and strong winds resulted in rapid cooling of the entire water column to just above 0 °C (Schindler et al. 1974), as in Ward Hunt Lake. Simulation of heat storage in Lake A, a meromictic lake near Ward Hunt Island, indicated that the loss of its perennial ice cover and exposure of its water column to the atmosphere could induce the loss of heat accumulated over more than 50 years, with eventual disappearance of its mid water column temperature maximum (Vincent et al. 2008). In Ward Hunt Lake in 2017, the persistence of lake ice in late summer allowed inverse stratification to be maintained, with warmer bottom water temperatures that continued into winter and spring. Similarly, in Colour Lake on Axel Heiberg Island, the persistence of late summer ice resulted in warmer temperatures beneath the ice in the subsequent spring than in years that followed a summer with ice-out, mixing and heat loss to the atmosphere (Doran et al. 1996).

The high frequency temperature record from summer 2016 indicated that the stratified waters beneath the ice contained strata of movement and mixing, including homogenous mid-water column temperatures that were suggestive of a sub-ice convection cell (as described in Pernica et al. 2017) and internal waves (Kirillin et al. 2012). After the period of cooling in the end of summer 2016, the bottom waters of the lake then rose in temperature during the period of early winter ice formation. This may be due to heat transfer from the sediments, but may also result from density flows of warmer water from the littoral zone that are enriched in ions due to salt exclusion by the forming moat ice or by sediment decomposition and mineralization processes (Cortés and MacIntyre 2020).

PAR and chlorophyll *a* fluorescence

The PAR regime of High Arctic lakes is constrained by the extreme seasonality of incident solar radiation, the persistence of thick ice throughout most of the year and the presence of overlying snow. The continuous in situ records from Ward Hunt Lake showed signs of combined effects of all three factors, which limited the period of under-ice PAR exposure to mostly July-August. The incident energy supply was almost identical for the two years, however the water column PAR differed sharply, with much lower irradiances in the lower water layer in August 2017 associated with the 2-year ice and its associated snow cover. The sharp increase in K_d during the late summer period of 2016 with strong winds and mixing suggests that this increased turbidity was due in large part to sediment resuspension, in combination with a rise in phytoplankton. The underwater PAR sensor at 9.0 m recorded values in the range 10 to 35 µmol photons m^{-2} s^{-1} from July to August in both years, which are above the thresholds for photosynthetic activity and biomass accrual (Gosselin et al. 1985). These values were at or above the PAR fluxes recorded under thick ice in McMurdo Dry Valley lakes; for example 3.5 µmol photons m^{-2} s^{-1} at 9.2 m depth in Lake Hoare when the ice cover was less than 4 m thick (Vopel and Hawes 2006), and 4 to 45 µmol photons m^{-2} s^{-1} at 10 m in Lake Bonney under 2 to 4 m of ice cover (Doran et al. 1996).

Two annual maxima in phytoplankton communities, one during spring mixing and the other during late summer-fall, are common in many north temperate lakes, although the pattern is often muted in oligotrophic waters (Kalff 2003). This bimodal pattern was also a feature of Ward Hunt Lake in both years. A spring peak in chlorophyll that developed beneath the ice followed by a late summer peak during and immediately after the open water period was also observed in Char Lake each year (Kalff and Welch 1974). The initial peak likely results from the use of nutrients released by mineralization over winter, while the second peak may be stimulated by nutrient inflows to the lake in late summer. Two periods of maximum phytoplankton densities have also been observed in Antarctic oligotrophic lakes, with highest chlorophyll *a* fluorescence recorded in fall (Tanabe et al. 2008).

The greater maximum chlorophyll *a* fluorescence in the late summer of 2016 versus 2017 may be the result of nutrient entrainment from the bottom waters and exposure to near surface light for photosynthesis during wind-induced mixing, in the absence of ice cover. Bioassays performed on samples from Ward Hunt Lake in summer indicated that the phytoplankton communities are highly responsive to nutrient input (Bonilla et al. 2005). The higher phytoplankton biomass suggested by the late summer fluorescence values in 2016 may also have influenced the subsequent nutrient and production regime in spring 2017, when higher fluorescence maxima were detected than in spring 2018. However, this potential legacy effect (Hampton et al. 2017) would require direct sampling and nutrient measurements to confirm.

The spring maximum in Ward Hunt Lake was delayed in 2017, likely because of the reduced light availability under the ice that year. Similarly in Char Lake, the spring increase was delayed during years of high snow cover (Kalff and Welch 1974). Snowfall is also a factor that is becoming more variable with climate warming in the Arctic, with extreme precipitation events observed recently

(Schmidt et al. 2019). Along with variable ice conditions, this will amplify the magnitude of interannual variability in energy supply for primary production.

The variations in chlorophyll *a* fluorescence measured in the mid water column provided an overall guide to the seasonal dynamics of phytoplankton biomass in Ward Hunt Lake, however this signal was almost certainly influenced by processes other than population growth. Large (up to 3 mm) visible colonies of the chrysophyte *Uroglena* along with other motile chrysophytes have been detected in this lake (Charvet et al. 2012). Some of the variations, and especially the sharp spikes observed in the high frequency record, may be due to large chrysophytes moving past the fluorescence sensor actively, given their known ability to actively migrate over the 24-h cycle (Paterson et al. 2008), or passively via vertical mixing. Changes in pigment concentrations per unit biomass are likely to take place over hours to days during physiological acclimation to changes in the ambient light regime, and over the longer term through photoadaptation (Moore et al. 2006), potentially leading to an overestimation of biomass from chlorophyll *a* under low light. Finally, in vivo chlorophyll *a* fluorescence is a complex physiological variable that is subject to multiple photoregulation processes at timescales from seconds to hours (Huot and Babin 2011). The rapid increase in signal during the snowfall event in late June 2017 may be the result of lower non-photochemical quenching of excitation energy in the dimmer light regime at that time, combined with upward migration of motile algal species from greater depths in the lake. The highest episodic peaks of chlorophyll *a* fluorescence, notably on 29 June 2017, thus have to be interpreted with caution, as they co-occurred with significantly lower irradiances (Fig. 2e). Excluding these sharp episodic peaks, and given the concordance between the fluorescence and HPLC values for chlorophyll *a* concentrations, the generally higher fluorescence values observed in late summer 2016 and the differences in timing of fluorescence maxima between years, imply that the interannual variation in ice-cover translated into effects on phytoplankton dynamics.

Oxygen dynamics

Despite the oligotrophic status of Ward Hunt Lake, its bottom waters showed marked seasonal variations in oxygen saturation, from anoxia to 140% of air-equilibrium. Oxygen accumulation below the ice is a common feature among ice-covered lakes (Craig et al. 1992). In addition to oxygen production by phytoplankton, cyanobacterial mats coat the bottom of Ward Hunt Lake and likely contribute to these seasonal variations (Mohit et al. 2017). Cyanobacteria-dominated mats in other systems have shown the potential to induce oxygen supersaturation in bottom waters (Vopel and Hawes 2006), and the microbial heterotrophs that occur abundantly in such mats (Mohit et al. 2017) may contribute to the oxygen draw-down in winter. Schindler et al. (1974) observed in Char Lake that even despite its extreme oligotrophic status, oxygen concentrations in its bottom waters fell to 2.5 mg L^{-1} (ca. 18% saturation) by the end of stratification, and attributed this to benthic respiration processes.

There were pronounced differences in the pattern of change in dissolved oxygen between the years with and without ice cover, as for the other limnological variables. During ice-off and mixing in 2016, the excess oxygen was ventilated to the atmosphere, but the water column remained oxic well into the early winter period. In 2017, the oxygen concentrations were rapidly depleted below air-equilibrium, and became anoxic in early winter, possibly because of higher sediment temperatures in 2017 versus the sediments in 2016 that had been cooled by water column mixing. The timing of switching from net oxygen accumulation to net depletion differed between years by a month. The oxygen sensor located at 8.5 m in 2016 was relocated at 9.3 m in 2017, which may have influenced the values recorded. However, this large difference in timing implies that the phytoplankton community was active longer in the absence of ice.

The observed rates of oxygen change expressed in absolute units of mg O_2 m^{-3} d^{-1} allow comparison with other waterbodies, and show that Ward Hunt Lake has sustained periods of net production or loss as a consequence of its active microbial communities under prolonged ice cover, and the annual light/dark cycle at high polar latitudes. The fastest net gains of 240-360 mg O_2 m^{-3} d^{-1} are comparable with rates over summer in Lake Hoare, Antarctica (e.g., net gain of 216 mg O_2 m^{-3} d^{-1} in the upper water column beneath 5 m of ice between 15 November 1980 and 22 January 1981; Wharton et al. 1986), where physical as well as biological processes have a controlling influence (Craig et al. 1992). These rates are well above net daily changes in the surface waters of lakes at temperate latitudes, where the gains from photosynthetic production over each 24 hour cycle may be approximately balanced by respiratory losses during the night-time hours of darkness, as well as by daily equilibration with the atmosphere (e.g., Fig. 2 in Staehr et al. 2010). The highest depletion rate observed in the lower water column of Ward Hunt Lake in 2017 (1067 mg O_2 m^{-3} $d^{-}1$) was similar to the most rapid losses recorded at the bottom of subarctic shallow thermokarst ponds in early winter (1060 mg O_2 m^{-3} d^{-1}; Deshpande et al. 2015). Application of a numerical model such as MyLake (Couture et al. 2015) to the high frequency data set from Ward Hunt Lake, once its morphometric, hydrological and hydrodynamic parameters are better defined, may allow further identification of biogeochemical processes controlling the large seasonal and interannual variability in oxygen concentrations, and the potential responses to ongoing change.

Conclusions

The High Arctic is moving into a new climate regime of not only warmer average air temperatures, but also an increasing amplitude of extreme weather. The long-term climate observations at Canada's far northern coast indicate a trend of increasing melting degree days since the 1990s, with

2016 as an anomalous year of extreme warming. The recent transition of Ward Hunt Lake from a regime of continuously thick multiannual ice to thinner ice that is vulnerable to full melt-out has made the lake especially sensitive to such extreme events. The complete loss of ice in 2016 resulted in a major disruption of the physicochemical dynamics of the lake. The lake became fully exposed to wind-induced mixing, which caused a rapid temperature decline, high turbidity and a longer period of oxygen fluctuations throughout fall and winter than during the subsequent year of persistent ice cover. These open water conditions were also accompanied by markedly higher chlorophyll *a* fluorescence values, suggesting an increase in phytoplankton biomass. These contrasting limnological conditions underscore the ecological importance of ice cover on polar lakes, and show how the combination of thinner ice and warming events can lead to an abrupt regime shift in ecosystem properties to a state of amplified year-to-year variability.

References

Babb, D. G., J. C. Landy, D. G. Barber, and R. J. Galley. 2019. Winter sea ice export from the Beaufort Sea as a preconditioning mechanism for enhanced summer melt: A case study of 2016. J. Geophys. Res. Oceans **124**: 6575–6600. doi:10.1029/2019JC015053

Belzile, C., W. F. Vincent, J. A. E. Gibson, and P. Van Hove. 2001. Bio-optical characteristics of the snow, ice, and water column of a perennially ice-covered lake in the High Arctic. Can. J. Fish. Aquat. Sci. **58**: 2405–2418. doi:10.1139/cjfas-58-12-2405

Bieniek, P. A., and J. E. Walsh. 2017. Atmospheric circulation patterns associated with monthly and daily temperature and precipitation extremes in Alaska. Int. J. Climatol. **37**: 208–217. doi:10.1002/joc.4994

Bonilla, S., V. Villeneuve, and W. F. Vincent. 2005. Benthic and planktonic algal communities in a High Arctic lake: Pigment structure and contrasting responses to nutrient enrichment. J. Phycol. **41**: 1120–1130. doi:10.1111/j.1529-8817.2005.00154.x

CEN. 2020. Climate station data from northern Ellesmere Island in Nunavut, Canada, v. 1.7 (2002-2019). Nordicana **D1**. doi:10.5885/44985SL-8F203FD3ACCD4138

Charvet, S., W. F. Vincent, and C. Lovejoy. 2012. Chrysophytes and other protists in High Arctic lakes: Molecular gene surveys, pigment signatures and microscopy. Polar Biol. **35**: 733–748. doi:10.1007/s00300-011-1118-7

Cortés, A., and S. MacIntyre. 2020. Mixing processes in small arctic lakes during spring. Limnol. Oceanogr. **65**: 260-288. doi:10.1002/lno.11296

Craig, H., R. A. Wharton, Jr., and C. P. McKay. 1992. Oxygen supersaturation in ice-covered Antarctic lakes: Biological versus physical contributions. Science **255**: 318–321. doi:10.1126/science.11539819

Couture, R.-M., H. A. de Wit, K. Tominaga, P. Kiuru, and I. Markelov. 2015. Oxygen dynamics in a boreal lake responds to long-term changes in climate, ice phenology, and DOC inputs. J. Geophys. Res. Biogeosci. **120**: 2441-2456. doi:10.1002/2015JG003065.

Deshpande, B., S. MacIntyre, A. Matveev, and W. F. Vincent. 2015. Oxygen dynamics in permafrost thaw lakes: Anaerobic bioreactors in the Canadian subarctic. Limnol. Oceanogr. **60**: 1656–1670. doi:10.1002/lno.10126

Doran, P. T., C. P. McKay, W. P. Adams, M. C. English, R. A. Wharton, Jr., and M. A. Meyer. 1996. Climate forcing and thermal feedback of residual lake-ice covers in the high Arctic. Limnol. Oceanogr. **41**: 839–848. doi:10.4319/lo.1996.41.5.0839

Du, J., J. S. Kimball, C. Duguay, Y. Kim, and J. D. Watts. 2017. Satellite microwave assessment of Northern Hemisphere lake ice phenology from 2002 to 2015. The Cryosphere **11**: 47–63. doi:10.5194/tc-11-47-2017

Fountain, A. G., and others. 2016. The impact of a large-scale climate event on Antarctic ecosystem processes. BioScience **66**: 848–863. doi:10.1093/biosci/biw110

Gosselin, M., L. Legendre, S. Demers, and R. G. Ingram. 1985. Responses of sea-ice microalgae to climatic and fortnightly tidal energy inputs (Manitounuk Sound, Hudson Bay). Can. J. Fish. Aquat. Sci. **42**: 999–1006. doi:10.1139/f85-125

Hampton, S. E., and others. 2017. Ecology under lake ice. Ecol. Lett. **20**: 98–111. doi:10.1111/ele.12699

Huot, Y., and M. Babin. 2011. Overview of fluorescence protocols: Theory, basic concepts, and practice, p. 31–74. *In* D.J. Suggett, O. Prášil, and M.A. Borowitzka [eds.], Chlorophyll *a* fluorescence in aquatic sciences: Methods and applications. Springer. doi:10.1007/978-90-481-9268-7_3

Kalff, J. 2003. Limnology: Inland water ecosystems. Prentice Hall.

Kalff, J., and H. E. Welch. 1974. Phytoplankton production in Char Lake, a natural polar lake, and in Meretta Lake, a polluted polar lake, Cornwallis Island, Northwest Territories. J. Fish. Res. Board Can. **31**: 621–636. doi:10.1139/f74-094

Kirillin, G., and others. 2012. Physics of seasonally ice-covered lakes: A review. Aquat. Sci. **74**: 659–682. doi:10.1007/s00027-012-0279-y

Landy, J. C., J. K. Ehn, and D. G. Barber. 2015. Albedo feedback enhanced by smoother Arctic sea ice. Geophys. Res. Lett. **42**: 10,714-10,720. doi:10.1002/2015GL066712

Lehnherr, I., and others. 2018. The world's largest High Arctic lake responds rapidly to climate warming. Nat. Commun. **9**: 1290. doi:10.1038/s41467-018-03685-z

Ludlam, S. D. 1996. The comparative limnology of high arctic, coastal, meromictic lakes. J. Paleolimnol. **16**: 111-131. doi:10.1007/BF00176931

Macias-Fauria, M., and E. Post. 2018. Effects of sea ice on Arctic biota: An emerging crisis discipline. Biol. Lett. **14**: 20170702. doi:10.1098/rsbl.2017.0702

Matveev, A., I. Laurion, and W. F. Vincent. 2019. Winter accumulation of methane and its variable timing of release from thermokarst lakes in subarctic peatlands. J. Geophys. Res. Biogeosci. **124**: 3521-3535. doi:10.1029/2019JG005078

Meredith, M., and others. 2019. Polar Regions, *In* H.-O. Pörtner and others [eds.], IPCC special report on the ocean and cryosphere in a changing climate. Intergovernmental Panel on Climate Change, World Meteorological Organization. https://www.ipcc.ch/srocc/

Mioduszewski, J. R., S. Vavrus, M. Wang, M. Holland, and L. Landrum. 2019. Past and future interannual variability in Arctic sea ice in coupled climate models. The Cryosphere **13**: 113–124. doi:10.5194/tc-13-113-2019

Mohit, V., A. Culley, C. Lovejoy, F. Bouchard, and W. F. Vincent. 2017. Hidden biofilms in a far northern lake and implications for the changing Arctic. npj Biofilms and Microbiomes **3**: 17. doi:10.1038/s41522-017-0024-3

Moore, C. M., and others. 2006. Phytoplankton photoacclimation and photoadaptation in response to environmental gradients in a shelf sea. Limnol. Oceanogr. **51**: 936-949. doi:10.4319/lo.2006.51.2.0936

Mudryk, L. R., and others. 2018. Canadian snow and sea ice: Historical trends and projections. The Cryosphere **12**: 1157–1176. doi:10.5194/tc-12-1157-2018

NEIGE. 2020. Dynamics of ice cover over a far northern lake: Direct observations of Ward Hunt Lake, Canadian High Arctic, by automated camera, v. 1.0 (2016-2018). Nordicana **D74**. doi:10.5885/45648CE-1A9AB63DFF91440B

Obryk, M. K., P. T. Doran, and J. C. Priscu. 2019. Prediction of ice-free conditions for a perennially ice-covered Antarctic lake. J. Geophys. Res. Earth Surf. **124**: 686–694. doi:10.1029/2018JF004756

Overland, J., and others. 2019. The urgency of Arctic change. Polar Sci. **21**: 6–13. doi:10.1016/j.polar.2018.11.008

Paquette, M., D. Fortier, D. R. Mueller, D. Sarrazin, and W. F. Vincent. 2015. Rapid disappearance of perennial ice on Canada's most northern lake. Geophys. Res. Lett. **42**: 1433–1440. doi:10.1002/2014GL062960

Paquette, M., D. Fortier, and W. F. Vincent. 2017. Water tracks in the High Arctic: A hydrological network dominated by rapid subsurface flow through patterned ground. Arct. Sci. **3**: 334–353. doi:10.1139/as-2016-0014

Paterson, A. M., and others. 2008. Long-term changes in phytoplankton composition in seven Canadian Shield lakes in response to multiple anthropogenic stressors. Can. J. Fish. Aquat. Sci. **65**: 846–861. doi:10.1139/f08-022

Pernica, P., R. L. North, and H. M. Baulch. 2017. In the cold light of day: the potential importance of under-ice convective mixed layers to primary producers. Inland Waters **7**: 138–150. doi:10.1080/20442041.2017.1296627

Sager, J. C., and J. C. McFarlane. 1997. Radiation, p. 1–29. *In* R.W. Langhans and T.W. Tibbitts [eds.], Plant growth chamber handbook. Iowa State University.

Schindler, D. W., H. E. Welch, J. Kalff, G. J. Brunskill, and N. Kritsch. 1974. Physical and chemical limnology of Char Lake, Cornwallis Island (75° N Lat.). J. Fish. Res. Board Can. **31**: 585–607. doi:10.1139/f74-092

Schmidt, N. M., J. Reneerkens, J. H. Christensen, M. Olesen, and T. Roslin. 2019. An ecosystem-wide reproductive failure with more snow in the Arctic. PLOS Biol. **17**: e3000392. doi:10.1371/journal.pbio.3000392

Schuur, E. A. G., and others. 2015. Climate change and the permafrost carbon feedback. Nature **520**: 171–179. doi:10.1038/nature14338

Serreze, M. C., and W. N. Meier. 2019. The Arctic's sea ice cover: Trends, variability, predictability, and comparisons to the Antarctic. Ann. N.Y. Acad. Sci. **1436**: 36–53. doi:10.1111/nyas.13856

Sharma, S., and others. 2019. Widespread loss of lake ice around the Northern Hemisphere in a warming world. Nat. Clim. Chang. **9**: 227–231. doi:10.1038/s41558-018-0393-5

Staehr, P. A., and others. 2010. Lake metabolism and the diel oxygen technique: State of the science. Limnol. Oceanogr. Methods **8**: 628-644. doi: 10.4319/lom.2010.8.0628

Tanabe, Y., S. Kudoh, S. Imura, and M. Fukuchi. 2008. Phytoplankton blooms under dim and cold conditions in freshwater lakes of East Antarctica. Polar Biol. **31**: 199–208. doi:10.1007/s00300-007-0347-2

Vincent, A. C., D. R. Mueller, and W. F. Vincent. 2008. Simulated heat storage in a perennially ice-covered high Arctic lake: Sensitivity to climate change. J. Geophys. Res. Oceans **113**: C04036. doi:10.1029/2007jc004360

Vincent, W.F. 2020. Arctic climate change: Local impacts, global consequences, and policy implications, p. 507-526. *In* K. S. Coates and C. Holroyd [eds.], The Palgrave handbook of Arctic policy and politics. Palgrave Macmillan, London. doi:10.1007/978-3-030-20557-7_31

Vincent, W. F., and others. 2011. Extreme ecosystems and geosystems in the Canadian High Arctic: Ward Hunt Island and vicinity. Ecoscience **18**: 236–261. doi:10.2980/18-3-3448

Vopel, K., and I. Hawes. 2006. Photosynthetic performance of benthic microbial mats in Lake Hoare, Antarctica. Limnol. Oceanogr. **51**: 1801–1812. doi:10.4319/lo.2006.51.4.1801

Wharton, R. A., Jr., C. P. McKay, G. M. Simmons, Jr., and B. C. Parker. 1986. Oxygen budget of a perennially ice-covered Antarctic lake. Limnol. Oceanogr. **31**: 437-443. doi:10.4319/lo.1986.31.2.0437

Wrona, F., and others. 2016. Transitions in Arctic ecosystems: Ecological implications of a changing hydrological regime. J. Geophys. Res. Biogeosci. **121**: 650–674. doi:10.1002/2015JG003133

Acknowledgements

This research is a contribution to the projects ArCS (Arctic Challenge for Sustainability) supported by the Ministry of Education, Culture, Sports, Science and Technology, Japan, and NEIGE (Northern Ellesmere Island in the Global Environment) supported by Sentinel North (Canada First , Research Excellence Fund), ArcticNet (NCE), CEN, Fonds de Recherche du Quebec Nature et Technologies (FRQNT), the Natural Sciences and Engineering Research Council of Canada (NSERC) and the Northern Scientific Training Program (NSTP), with logistic support from the Polar Continental Shelf Program (PCSP) and Parks Canada. This work is also a contribution to the International Arctic Science Committee (IASC) project T-MOSAiC (Terrestrial Multidisciplinary distributed Observatories for the Study of Arctic Connections). The authors would also like to thank Myriam Labbé, Jérôme Comte and Nicolas Bochaton for their help with fieldwork and two anonymous reviewers for their insightful comments and suggestions that improved the manuscript.

Figure legends

Figure 1. Melting degree days at Ward Hunt Island (bars) and Alert (black line and points). The arrows mark 2016, the year of extreme warming. The red lines are the overall average values for the two records.

Figure 2. Data collected by the mooring in Ward Hunt Lake from 20 July 2016 to 19 July 2018 and at the Ward Hunt Island climate station. a) Water temperatures at eight depths (this is replotted as a heat map in Supporting Information Fig. S3); b) Air temperature; c) Photosynthetically active radiation (PAR) in the air; d) PAR in the upper water (2.8 m; red line) and lower water column (8.5 m; black line); e) Chlorophyll *a* (Chl *a*) fluorescence (green line) and concentration measured by HPLC (black points) in the middle of the water column (5.8 m); and f) Dissolved oxygen concentrations as % air-equilibrium in the lower (8.5 m) water column in 2016 and in the upper (3.8 m), middle (5.8 m) and lower (9.3 m) water column in 2017. The blue shadow corresponds to the ice-free period (from ice break-up to new ice formation) in summer 2016. The gray shadows correspond to date intervals used to calculate the linear net oxygen change rates in the lower layer of the water column (Table 1).

Figure 3. Temperature (black) and oxygen (red) in the deep layer (8.5 m) of Ward Hunt Lake during four summers. The blue shadow corresponds to the ice-free period (from ice break-up to new ice formation) in summer 2016. Letters represent major events in ice phenology in 2016: a) ice cover break-up, b) ice-free conditions, c) new ice formation, d) thick ice formation. Corresponding dates in 2017: e) ice cover thinning, f) snow accumulation on ice cover, g) new ice formation in the moat, h) thick ice formation.

Figure 4. Mean daily values of photosynthetically active radiation (PAR) and chlorophyll *a* (Chl *a*) fluorescence. PAR a) in air; b) in the upper (2.8 m) and c) lower water column (8.5 m); and d) chlorophyll *a* fluorescence in the middle water column (5.8 m) of Ward Hunt Lake. The blue shadow corresponds to the ice-free period (from ice break-up to new ice formation) in summer 2016.

Figure 5. Comparison attenuation coefficients (K_d) between years. Hourly data are shown for the periods: a) from 30 July to 30 August; and b) from 5 June to 15 July. The coefficients were calculated from the in situ irradiance measurements at 2.8 and 8.5 m.

Tables

Extreme warming and regime shift to amplified variability in a far northern lake

P. N. Bégin, Y. Tanabe, M. Kumagai, A. I. Culley, M. Paquette, D. Sarrazin, M. Uchida and W. F. Vincent

Table 1. Linear oxygen change rates in Ward Hunt Lake. The values are expressed in terms of net increase or decrease in oxygen saturation (% air-equilibrium) per unit time. The numbers refer to the periods identified by gray shadows in Fig. 2f.

	Time period	Net oxygen change rate (% d^{-1})		
		3.8 m	5.8 m	Bottom[a]
	2016			
1	21-25 July	-	-	5.31
2	30 July - 7 August	-	-	-2.30
3	7 August - 17 September	-	-	0.08
4	17 September - 3 October	-	-	-3.03
	2017			
5	23 July - 14 August 2017	-1.44	-0.17	2.48
6	15 August - 5 September 2017	-2.86[b]	-7.89[c]	-1.85
7	5 - 9 September 2017	0.09	-0.05	-14.57
8	9 -20 October 2017	0.03	-1.8	<0.001
	2018			
9	29 June - 10 July 2018	0.62	5.10	<0.001
10	10 - 20 July 2018	1.17	0.81	<0.001

[a] 8.5 m in 2016 and 9.3 m in 2017; [b]15 to 18 August 2017; [c]15 to 19 August 2017

- no data

Table 2. Net oxygen change rates in Ward Hunt Lake for equivalent 2-week time periods in 2016 and 2017.

Time period	Net oxygen change rate (mg O_2 m^{-3} d^{-1})			
	2017			2016
	3.8 m	5.8 m	9.3 m	8.5 m
20-31 July	-4.1	+16.5	+240.9	+358.6
01-15 August	-100.8	-32.1	+236.7	+10.5
16-31 August	-18.2	-144.3	-192.5	+6.2
01-15 September	7.4	-7.2	-1067.4	+16.2
16-30 September	-3.2	-7.6	-60.0	-477.1
01-15 October	+6.8	-102.2	+0.1	-221.4
16-31 October	+5.0	-31.3	+0.1	-89.9

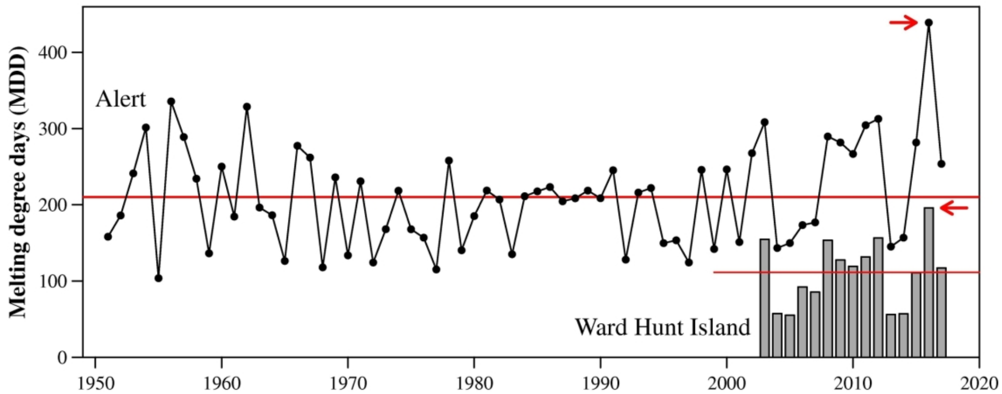

Figure 1. Melting degree days at Ward Hunt Island (bars) and Alert (black line and points). The arrows mark 2016, the year of extreme warming. The red lines are the overall average values for the two records.

184x76mm (300 x 300 DPI)

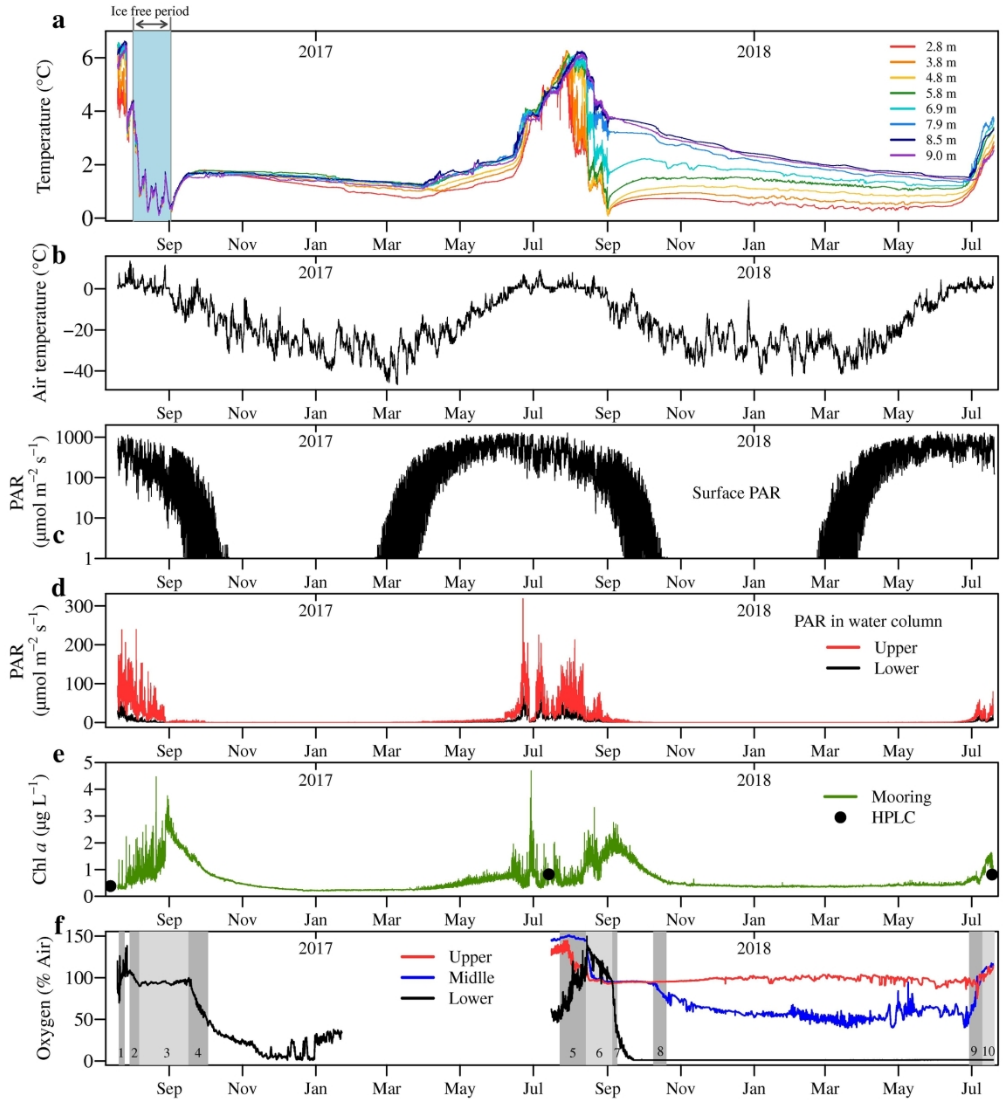

Figure 2. Data collected by the mooring in Ward Hunt Lake from 20 July 2016 to 19 July 2018 and at the Ward Hunt Island climate station. a) Water temperatures at eight depths (this is replotted as a heat map in Supporting Information Fig. S3); b) Air temperature; c) Photosynthetically active radiation (PAR) in the air; d) PAR in the upper water (2.8 m; red line) and lower water column (8.5 m; black line); e) Chlorophyll *a* (Chl *a*) fluorescence (green line) and concentration measured by HPLC (black points) in the middle of the water column (5.8 m); and f) Dissolved oxygen concentrations as % air-equilibrium in the lower (8.5 m) water column in 2016 and in the upper (3.8 m), middle (5.8 m) and lower (9.3 m) water column in 2017. The blue shadow corresponds to the ice-free period (from ice break-up to new ice formation) in summer 2016. The gray shadows correspond to date intervals used to calculate the linear net oxygen change rates in the lower layer of the water column (Table 1).

184x203mm (300 x 300 DPI)

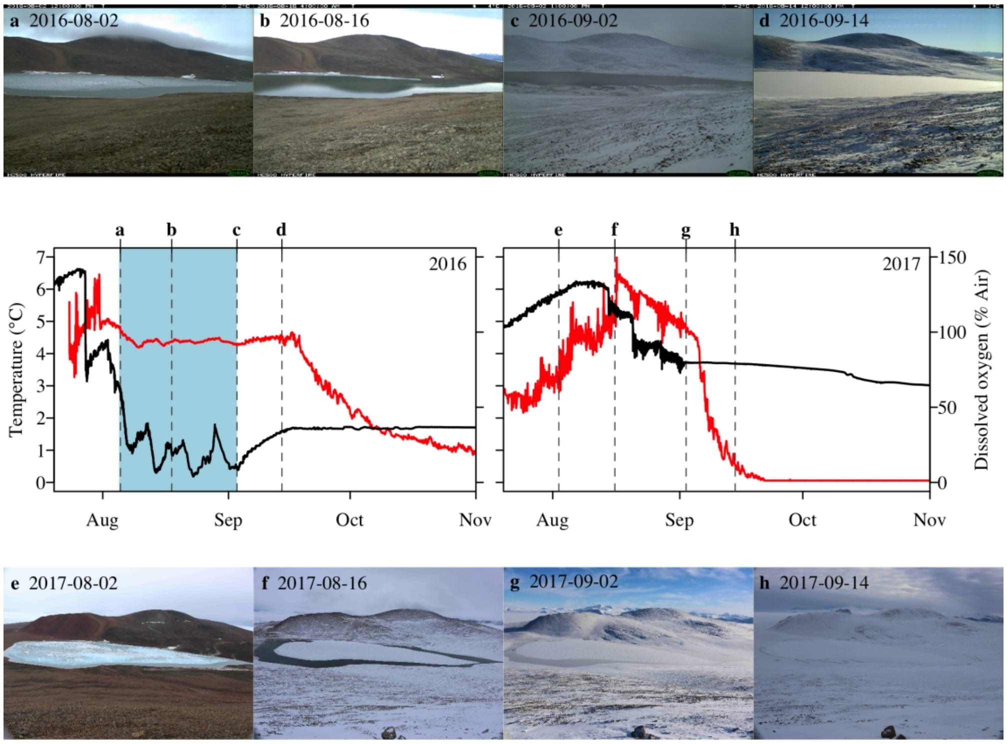

Figure 3. Temperature (black) and oxygen (red) in the deep layer (8.5 m) of Ward Hunt Lake during four summers. The blue shadow corresponds to the ice-free period (from ice break-up to new ice formation) in summer 2016. Letters represent major events in ice phenology in 2016: a) ice cover break-up, b) ice-free conditions, c) new ice formation, d) thick ice formation. Corresponding dates in 2017: e) ice cover thinning, f) snow accumulation on ice cover, g) new ice formation in the moat, h) thick ice formation.

767x582mm (72 x 72 DPI)

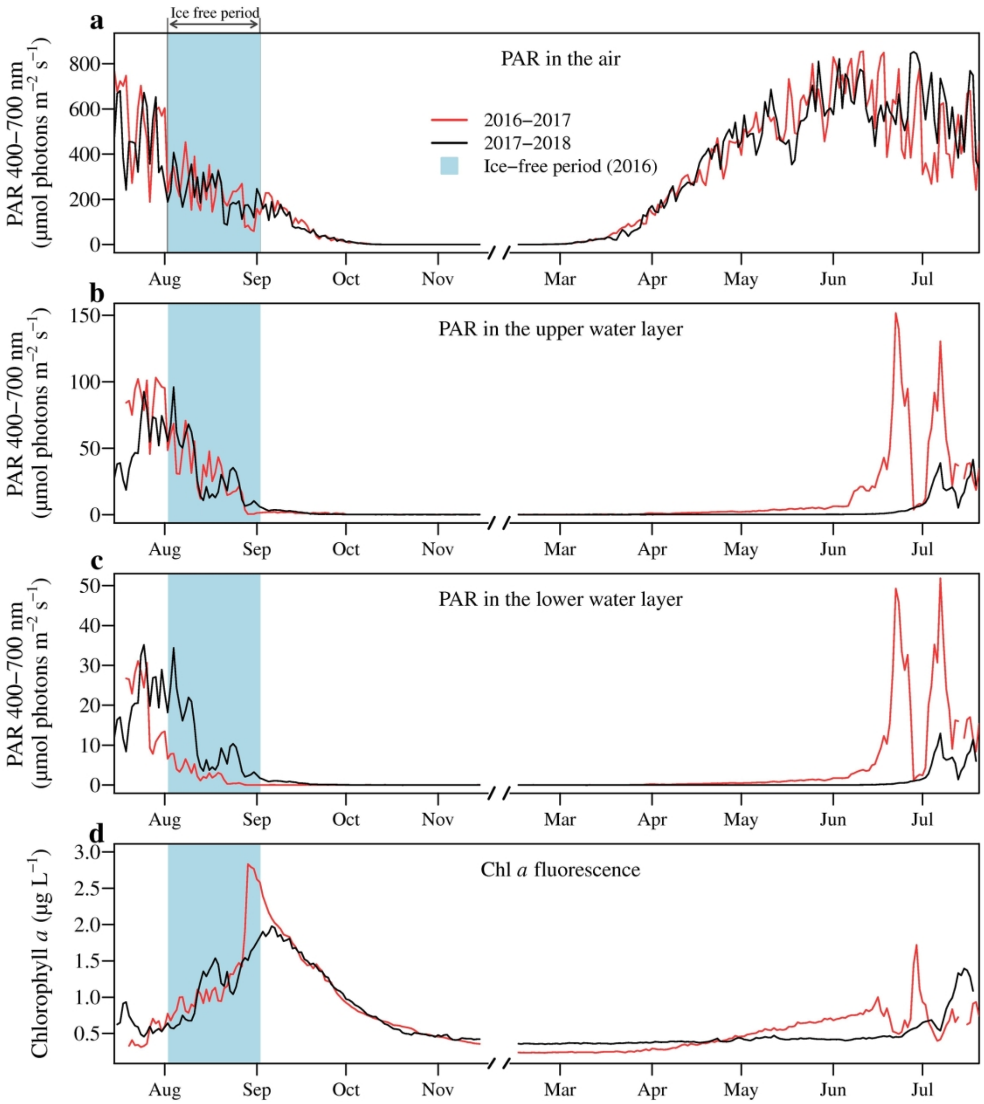

Figure 4. Mean daily values of photosynthetically active radiation (PAR) and chlorophyll *a* (Chl *a*) fluorescence. PAR a) in air; b) in the upper (2.8 m) and c) lower water column (8.5 m); and d) chlorophyll *a* fluorescence in the middle water column (5.8 m) of Ward Hunt Lake. The blue shadow corresponds to the ice-free period (from ice break-up to new ice formation) in summer 2016.

184x203mm (300 x 300 DPI)

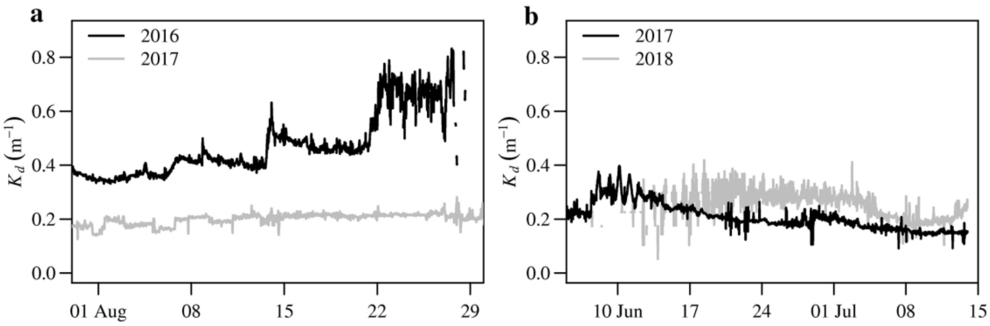

Figure 5. Comparison attenuation coefficients (K_d) between years. Hourly data are shown for the periods: a) from 30 July to 30 August; and b) from 5 June to 15 July. The coefficients were calculated from the in situ irradiance measurements at 2.8 and 8.5 m.

184x63mm (300 x 300 DPI)

Supporting Information

Extreme warming and regime shift toward amplified variability in a far northern lake

P. N. Bégin, Y. Tanabe, M. Kumagai, A. I. Culley, M. Paquette, D. Sarrazin, M. Uchida and W. F. Vincent

Table S1. Air temperature, freezing degree days and incoming radiation on Ward Hunt Island, Nunavut.

Month	Annual values																**Means**
	2003	2004	2005	2006	2007	2008	2009	2010	2011	2012	2013	2014	2015	2016	2017	2018	2003 to 2017
Air temperature (°C) [a]																	
Jan.	-30.1	-34.8	-31.3	-29.8	-30.3	-36.1	-27.2*	-32.0	-28.1*	-30.6	-29.1	-31.4	-30.7	-27.9*	-29.9	-27.7*	**-30.6**
Feb.	-35.2	-35.0	-28.8*	-32.8	-30.8	-30.1	-33.2	-30.4	-34.0	-31.9	-38.5	-30.6	-30.0	-28.9*	-30.6	-28.6*	**-32.0**
March	-35.5	-39.9	-32.7	-29.9	-33.8	-36.6	-37.5	-30.9	-26.5*	-34.1	-29.7	-29.7	-33.3	-30.8	-31.0	-31.4	**-32.8**
April	-25.0	-25.0	-25.5	-21.0*	-20.2*	-24.7	-25.8	-17.4*	-26.8	-22.9	-23.4	-22.2	-22.7	-24.8	-22.7	-25.3	**-23.3**
May	-10.8	-12.0	-9.1	-7.6*	-12.6	-9.3	-10.2	-8.0*	-10.2	-10.8	-11.8	-8.8*	-12.9	-10.0	-11.5	-11.1	**-10.4**
June	-1.6	-1.1	-0.7	-0.9	-0.7	1.0*	-1.7	-0.1	1.3*	1.2*	-1.5	-1.7	-0.1	1.3*	-0.8	-1.1	**-0.4**
July	2.9*	0.9	1.1	1.6	0.9	1.7	2.3	2.5	1.3	2.2	0.9	0.4	2.0	3.2*	1.7	NA	**1.7**
Aug.	1.1*	0.2	-1.0	-0.8	0.4	-0.7	0.7	-0.3	0.3	0.4	-3.0	-0.3	-0.5	1.2*	-0.4	NA	**-0.2**
Sept.	-6.7	-11.9	-8.7	-5.3*	-6.6	-8.4	-6.9	-9.3	-9.7	-8.3	-10.5	-6.8	-7.4	-6.7	-10.8	NA	**-8.3**
Oct.	-17.9	-21.0	-19.7	-14.3*	-18.2	-21.2	-18.6	-16.1*	-20.2	-17.8	-18.7	-18.3	-17.4	-16.4*	-20.8	NA	**-18.4**
Nov.	-29.3	-29.6	-25.9	-25.5	-28.5	-22.6*	-22.1*	-22.4*	-23.6	-25.9	-24.4	-25.8	-24.2	-21.7*	-27.4	NA	**-25.3**
Dec.	-29.0	-34.0	-27.9	-32.6	-28.0	-29.5	-27.0	-25.5*	-31.4	-27.0	-29.5	-29.6	-31.7	-25.1*	-25.3*	NA	**-28.9**
Annual mean	**-18.1**	**-20.3**	**-17.5**	**-16.6**	**-17.4**	**-18.0**	**-17.3**	**-15.8***	**-17.3**	**-17.1**	**-18.3**	**-17.1**	**-17.4**	**-15.6***	**-17.5**	**Inc.**	**-17.4**
Freezing degree days [b]																	
Total	Inc.	7040	6828	6291	6397	6774	6728	5994*	6084*	6648	6550	6498	6460	6304	6054*	6394	**6470**

Data from the Nordicana D archive (CEN 2020). NA: not available; Inc.: incomplete data.

[a] Based on hourly measurements. *Values exceeded the mean by more than 1 SD.

[b] Totals are from July of the previous year to June of the listed year. *Values were lower than mean by more than 1 SD.

Table S2. Air temperature and freezing degree days at Alert, Nunavut.

Month	Annual values																		**Means**
	2001	2002	2003	2004	2005	2006	2007	2008	2009	2010	2011	2012	2013	2014	2015	2016	2017	2018	**2003–2017**
Air temperature (°C) [a]																			
Jan.	-31.5	-32.7	-28.8	-33.0	-31.7	-27.5*	-29.0	-32.6	-26.9*	-29.5	-26.3*	-30.0	-28.4*	-27.7*	-26.9*	-24.0**	-29.1	-27.5*	**-31.5**
Feb.	-34.7	-39.2	-34.6	-33.2	-27.3*	-31.3	-28.1*	-27.4*	-30.9	-28.1*	-30.2	-30.9	-37.3	-29.0*	-29.4*	-27.4*	-28.7*	-24.8**	**-32.8**
March	-35.3	-32.5	-36.4	-36.8	-31.8	-28.0*	-31.9	-32.4	-34.4	-28.4*	-25.2**	-32.1	-27.9*	-27.6*	-30.5	-29.4*	-30.2	-29.3*	**-32.3**
April	-26.3	-28.0	-26.2	-24.5	-25.6	-20.4*	-19.4*	-23.3	-25.1	-18.5*	-25.8	-23.4	-22.6	-18.9*	-22.5	-24.5	-22.8	-24.4	**-24.2**
May	-14.2	-12.3	-12.0	-12.9	-8.4*	-8.0*	-13.2	-10.0	-10.9	-8.1*	-9.4	-11.2	-11.7	-9.3	-14.1	-11.4	-11.9	-11.8	**-11.5**
June	-0.9	-0.1	-1.5	-1.5	0.6	-0.6	-0.1	1.7*	-2.4	-0.2	2.9**	2.0*	-0.2	-2.2	1.4*	2.9**	0.1	-0.8	**-0.5**
July	2.6	4.0	5.8*	2.9	2.7	3.7	2.4	4.6	5.3*	5.5*	2.9	4.3	2.4	1.8	5.5*	8.1***	4.4	3.8	**3.6**
Aug.	0.8	3.2*	2.6*	0.9	-0.5	-0.2	1.6	0.3	3.1*	1.4	3.0*	3.0*	-1.1	2.5*	0.2	2.3*	1.6	3.0*	**1.0**
Sept.	-8.8	-7.4	-6.1*	-11.7	-8.6	-5.5*	-6.0*	-8.4	-6.2*	-9.9	-8.0	-7.2	-8.9	-7.2	-7.1*	-4.6**	-9.9	-8.0	**-9.1**
Oct.	-18.7	-13.5**	-17.2	-20.9	-18.3	-12.5**	-15.6*	-18.0	-17.4	-18.2	-17.9	-16.2*	-18.1	-17.6	-15.3*	-14.7*	-20.1	-13.9*	**-18.8**
Nov.	-26.0	-25.5	-27.9	-29.0	-25.3	-24.0	-23.9	-21.8*	-20.6*	-22.1*	-22.3*	-23.6	-24.5	-23.9	-22.9	-18.9**	-24.6	NA	**-25.7**
Dec.	-25.4*	-25.6*	-28.2	-33.3	-26.0*	-30.0	-27.1	-28.2	-25.0*	-23.4**	-28.9	-24.0*	-26.8	-27.2	-26.4	-24.9*	-25.8*	NA	**-29.1**
Annual mean	**-18.1**	**-17.3**	**-17.4**	**-19.4**	**-16.6**	**-15.4***	**-15.8***	**-16.3**	**-15.8***	**-14.9****	**-15.3***	**-15.7***	**-17.0**	**-15.4***	**-15.6***	**-13.8*****	**-16.3**	**Inc.**	**-17.5**
Freezing degree days [b]																			
Total	6990	6810	6439	6753	6703	5932*	5962*	6093*	6324	5550**	5795**	6266	6045*	5948*	6082*	5779**	5679**	6084*	**6597**

Data collected by Environment Canada (data available at http://climate.weather.gc.ca). NA: Not available, Inc.: incomplete data.

[a] Based on hourly measurements. Asterisked values exceeded the mean by more than 1 (*), 2 (**) or 3 (***) SD.

[b] Totals are from July of the previous year to June of the listed year. Asterisked values were lower than the mean by more than 1 (*) or 2 (**) SD.

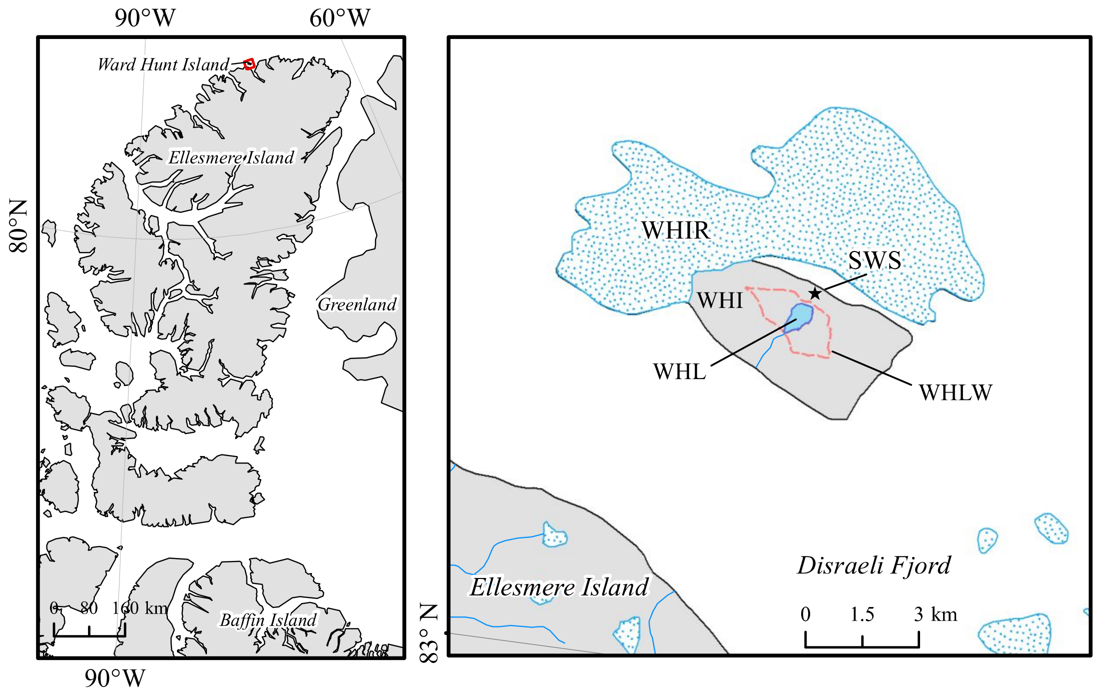

Fig. S1. Map of the study region. WHIR: Ward Hunt Ice Rise; WHI: Ward Hunt Island; WHL: Ward Hunt Lake; WHLW: Ward Hunt Lake watershed; SWS: SILA weather station.

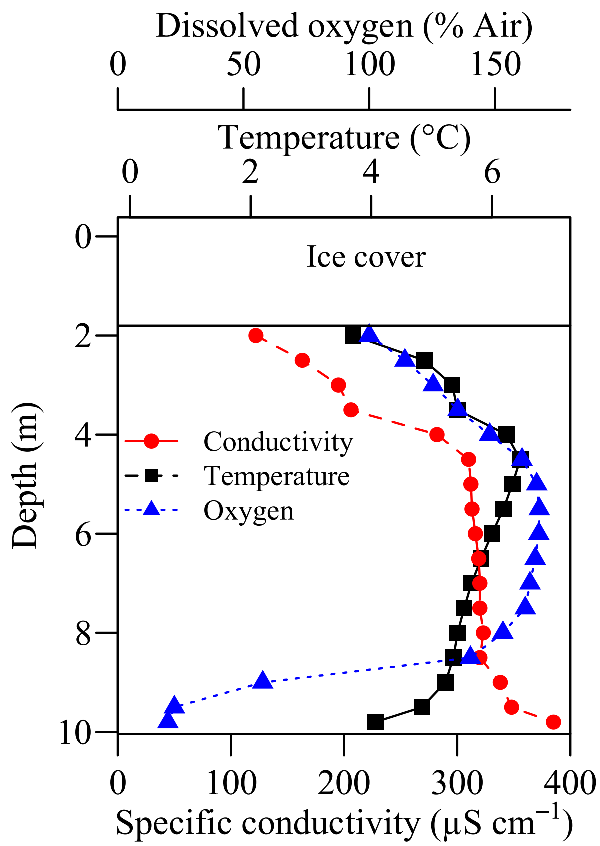

Fig. S2. Specific conductivity, water temperature and dissolved oxygen profiles (% saturation) at the deepest point of Ward Hunt Lake, 14 July 2016, under a 180 cm ice cover. The measurements were obtained with a YSI 600QS profiler (YSI Inc., OH, USA)

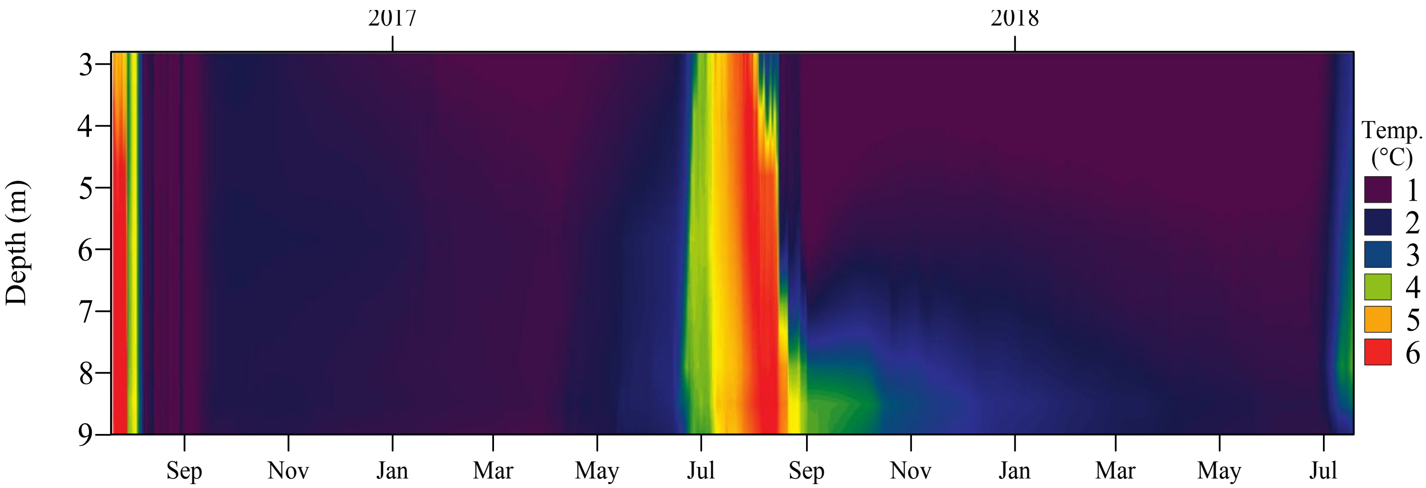

Fig. S3. Heatmap plot of water temperature changes in Ward Hunt Lake from 20 July 2016 to 19 July 2018.

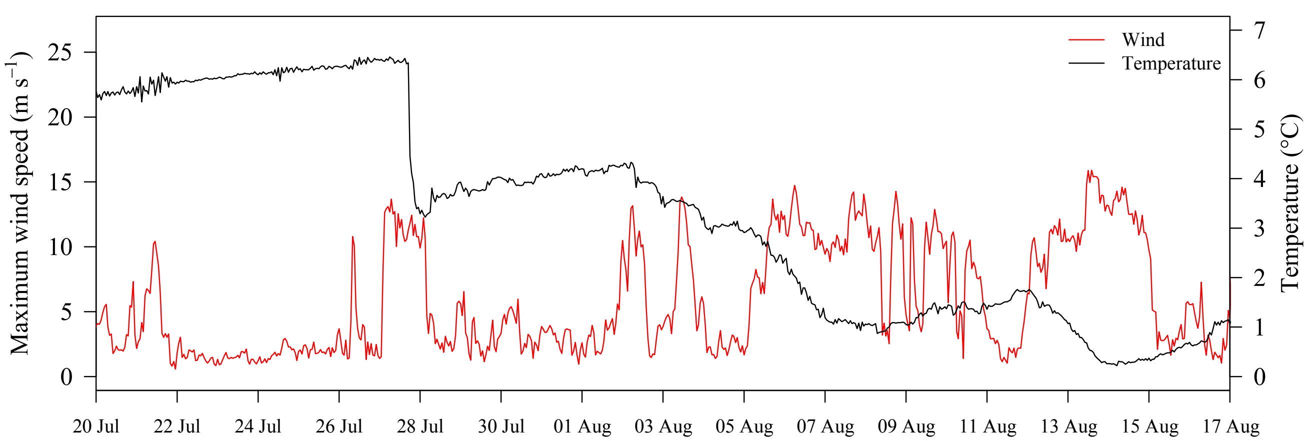

Fig. S4. Changes in daily maximum wind speed at the SILA station (10 m height) and temperature of the water at 9.0 m in July and August 2016.

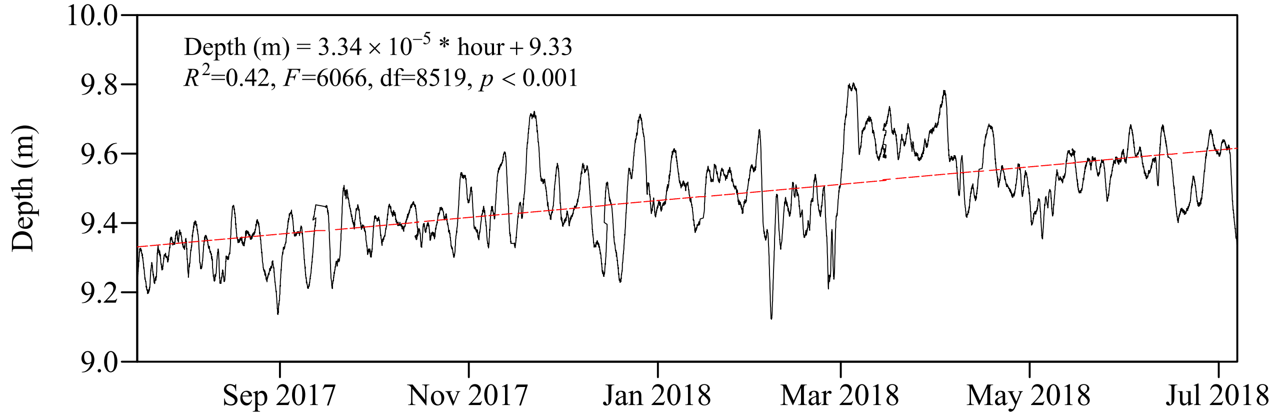

Fig. S5. Depth recorded by the logging CTD installed at 9.3 m from 15 July 2017 to 9 July 2018. The red dashed line is the the curve fitted by linear regression (details inserted in the figure).

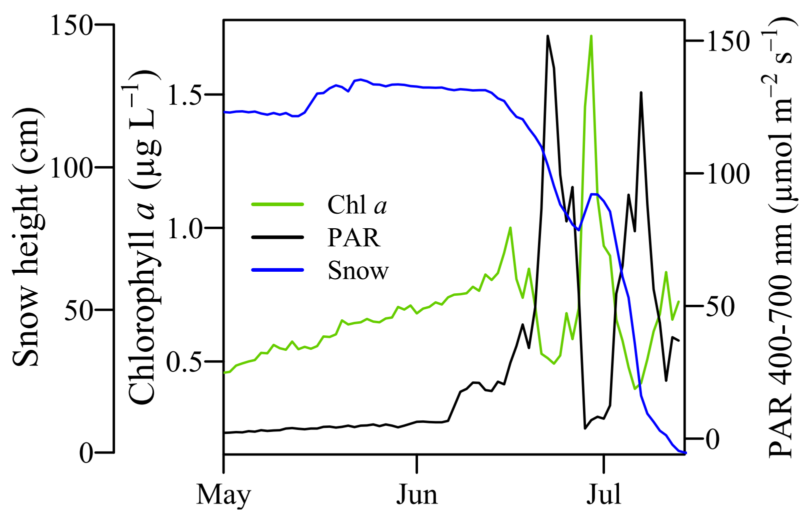

Figure S6. Chlorophyll *a* (Chl *a*) fluorescence at 5.8 m depth, photosynthetically active radiation (PAR) at the surface of Ward Hunt Lake and snow accumulation on the ground at the SILA station from 1 May to 14 July 2017.

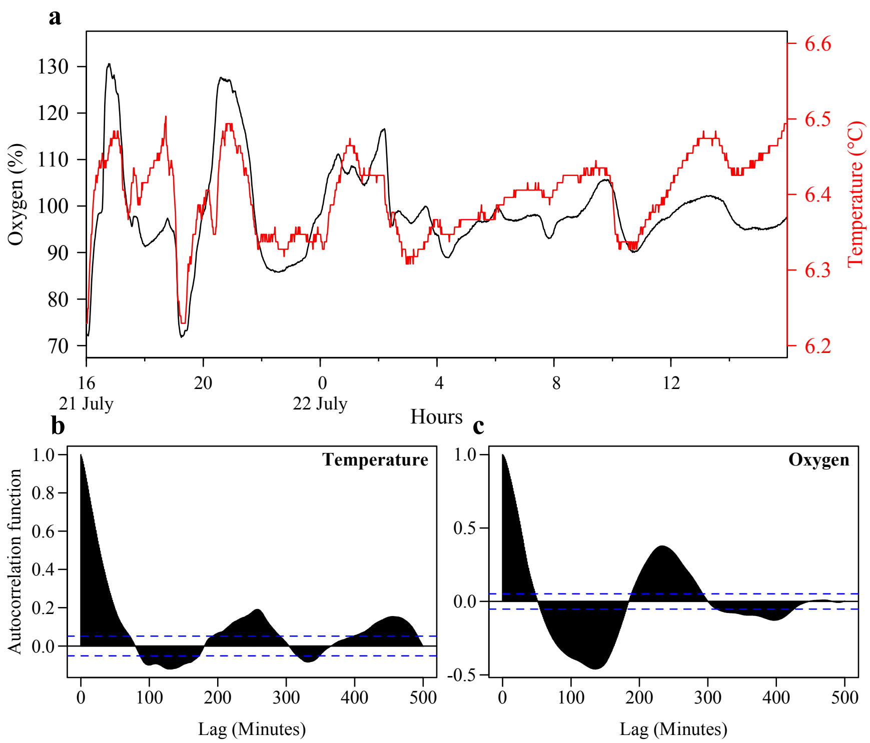

Fig. S7. Dissolved oxygen saturation at 8.5 m from 21 to 22 July 2016, following a strong wind event (Fig. S4). a) Oxygen (black line) and temperature (red line) changes at 1-min intervals through time. b) Autocorrelation function for temperature. c) Autocorrelation function for dissolved oxygen. Autocorrelation functions were performed with the *acf* function in *R*.